ACS APPLIED ENERGY MATERIALS
Cite This: ACS Appl. Energy Mater. 2018, 1, 3013−3018
Letter
www.acsaem.org

Cluster Beam Deposition of Ultrafine Cobalt and Ruthenium Clusters for Efficient and Stable Oxygen Evolution Reaction

Junyuan Xu,[†] Shane Murphy,[‡,#] Dehua Xiong,[†,▽] Rongsheng Cai,[‡,§] Xian-Kui Wei,[∥] Marc Heggen,[∥] Emanuele Barborini,[⊥] Simone Vinati,[⊥] Rafal E. Dunin-Borkowski,[∥] Richard E. Palmer,*[,§] and Lifeng Liu*[,†]

[†]International Iberian Nanotechnology Laboratory (INL), 4715-330 Braga, Portugal

[‡]Nanoscale Physics Research Laboratory, School of Physics and Astronomy, University of Birmingham, Birmingham B15 2TT, United Kingdom

[§]College of Engineering, Swansea University, Bay Campus, Fabian Way, Swansea SA1 8EN, United Kingdom

[∥]Ernst Ruska-Centre for Microscopy and Spectroscopy with Electrons and Peter Grünberg Institute, Forschungszentrum Jülich GmbH, 52425 Jülich, Germany

[⊥]Tethis S.p.A., via Russoli 3, 20143 Milano, Italy

Supporting Information

ABSTRACT: Ultrafine cobalt and ruthenium clusters are deposited on carbon paper substrates by cluster beam deposition using a matrix assembly cluster source and a pulsed microplasma cluster source, respectively. When used to catalyze the oxygen evolution reaction (OER), the cobalt and ruthenium clusters show electrocatalytic performance superior to the state-of-the-art Ru/C and RuO_2 nanoparticle catalysts on both a mass and a specific-surface-area basis. Typically, the cobalt clusters can deliver 10 mA cm^{-2} at a low overpotential of 320 mV and show a small Tafel slope of 50 mV dec^{-1} and a mass-based turnover frequency of 0.01 s^{-1} at an overpotential of 300 mV, outperforming many cobalt-based OER catalysts.

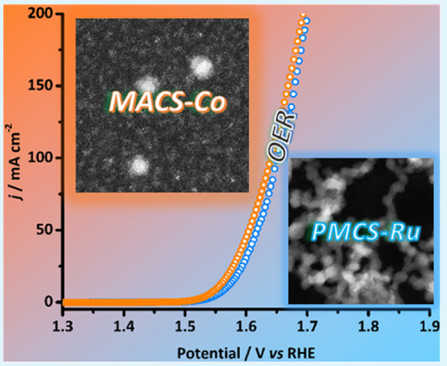

KEYWORDS: *cluster beam deposition, cobalt nanoparticles, ruthenium nanoparticles, electrocatalysis, oxygen evolution reaction*

Converting off-peak renewable energy (e.g., solar, wind) to clean and storable hydrogen (H_2) fuel through water splitting has been proposed as a promising and sustainable approach to renewable energy storage on a large scale, commensurate with future global demand.[1] Water splitting involves two half-cell reactions, namely, the hydrogen evolution reaction (HER) at the cathode and the oxygen evolution reaction (OER) at the anode. Presently, one of the key challenges for widespread deployment of water electrolyzers is to develop efficient, low-cost, and durable electrocatalysts to make electrolyzed H_2 fuel economically competitive over the H_2 produced by steam reforming of natural gas.[2] While the cathodic HER can usually occur at a relatively small overpotential, the anodic OER is much more difficult to accomplish, because it involves four concerted proton-coupled electron transfer steps and requires a large overpotential to take place at a practically useful rate, which may lead to notable energy losses. To overcome this bottleneck, considerable research efforts have been recently dedicated to the development of cost-effective earth-abundant OER electrocatalysts as well as to improving the utilization of noble metal catalysts by reducing their sizes or alloying with non-noble metal elements.[2−10]

Although a variety of methods have been developed to prepare nanoscale electrocatalysts, few of them allow for the synthesis of ultrafine clusters with controllable sizes. To this end, cluster beam deposition (CBD)[11] has proven to be a powerful technique for electrocatalyst preparation,[12,13] with the potential to offer unparalleled control over cluster size (e.g., with mass-filtering one can control the cluster size with even single-atom precision[14,15]) and the ability to deposit pristine clusters that are free of the ligands associated with "wet" synthesis. Moreover, CBD also offers the possibility to "pin" clusters to their support, making them more robust against sintering, by accelerating ionized clusters in an electric field toward the substrate.[16] In addition, CBD provides a rapid route to investigating new alloy clusters[17] compared to chemical synthesis routes and can be considered a more environmentally

Received: January 26, 2018
Accepted: June 11, 2018
Published: June 11, 2018

DOI: 10.1021/acsaem.8b00111
ACS Appl. Energy Mater. 2018, 1, 3013−3018

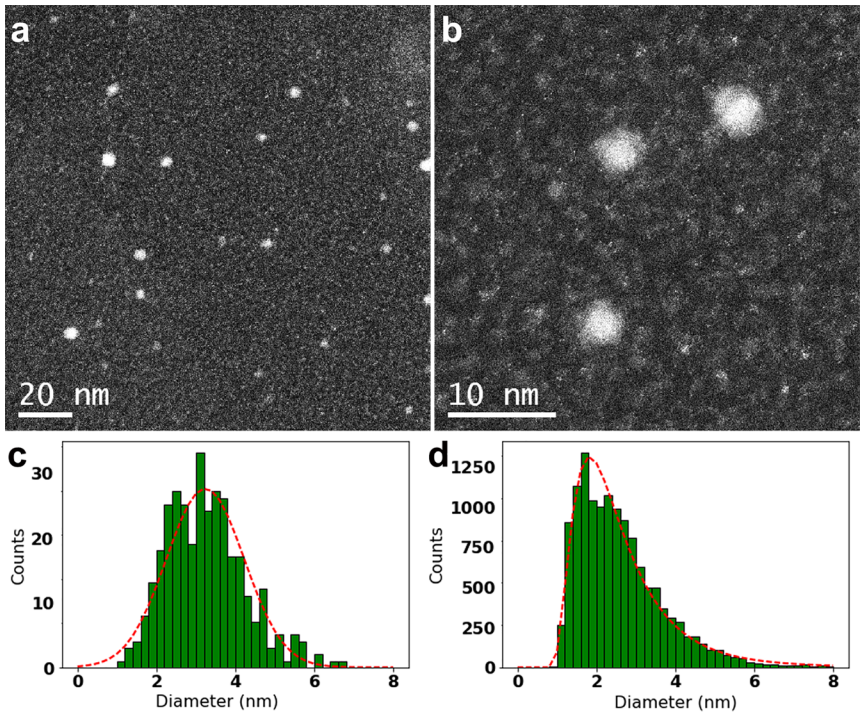

Figure 1. HAADF-STEM images of Co clusters, (a) 157 nm × 157 nm and (b) 39 nm × 39 nm, prepared by MACS for 40 min showing a bimodal ensemble comprising a low coverage of large clusters with a mean diameter of 3.2 ± 1.0 nm, surrounded by a high density of smaller clusters with a mean diameter of 1.8 ± 0.8 nm. The number of small clusters per unit area far exceeds that of the larger clusters. Consequently, separate particle size distributions are displayed for each cluster type, determined by threshold analysis at different magnifications, which are shown in panels c and d.

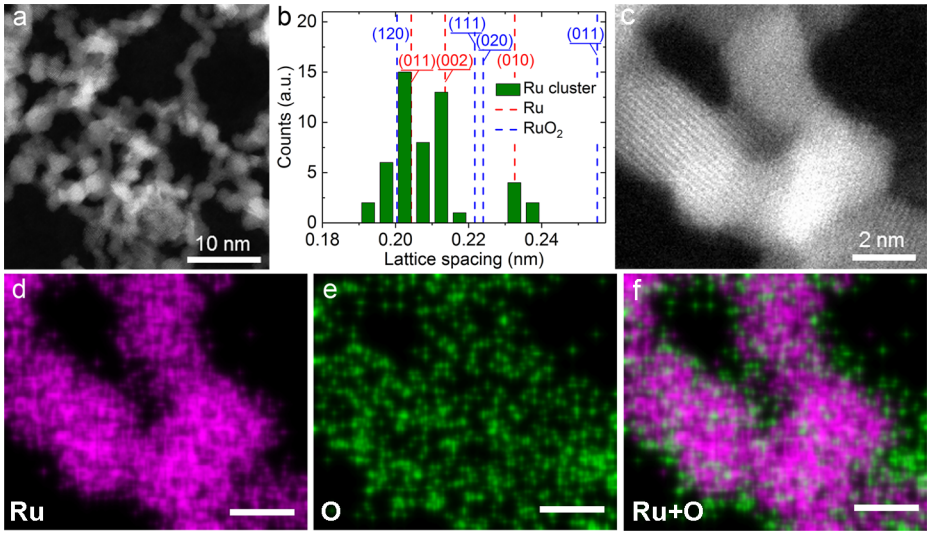

Figure 2. (a) HAADF-STEM image of Ru clusters. (b) Histogram showing the distribution of measured lattice spacing upon the HR-STEM image analyses. Comparison with the lattice spacing of metallic Ru and RuO_2 confirms the metallic nature of the deposited Ru clusters. (c) High-resolution HAADF-STEM image of local clusters. Elemental maps of (d) Ru, (e) O, and (f) their overlay. Scale bars: 2 nm.

benign technique as it does not involve potentially harmful reagents or byproducts.

In this work, two CBD approaches are adopted to deposit cobalt (Co) and ruthenium (Ru) cluster catalysts, respectively, on carbon paper (CP) substrates for use to catalyze the OER. First, a new high-yield CBD approach, based on the matrix assembly cluster source (MACS), in which clusters are produced by sputtering of a cryogenic gas-metal matrix,[18−21] was used to prepare ultrafine Co clusters (MACS-Co). Control over the cluster size is achieved through selection of the matrix composition (metal loading), temperature, and sputtering parameters. As a result, a high flux of size-controlled clusters (of the order of 30−45% in diameter) can be deposited without the need for a subsequent mass-filtering step, which would inevitably lead to loss of material. Second, the pulsed microplasma cluster source (PMCS)[22,23] was utilized to deposit Ru clusters (PMCS-Ru). PMCS allows for direct deposition of a cluster-assembled, uniform and nanoporous layer on the substrates of interest. The coverage uniformity is achieved by rastering the substrates in front of the cluster beam. For the present study, cluster-assembled Ru samples having basically

DOI: 10.1021/acsaem.8b00111
ACS Appl. Energy Mater. 2018, 1, 3013−3018

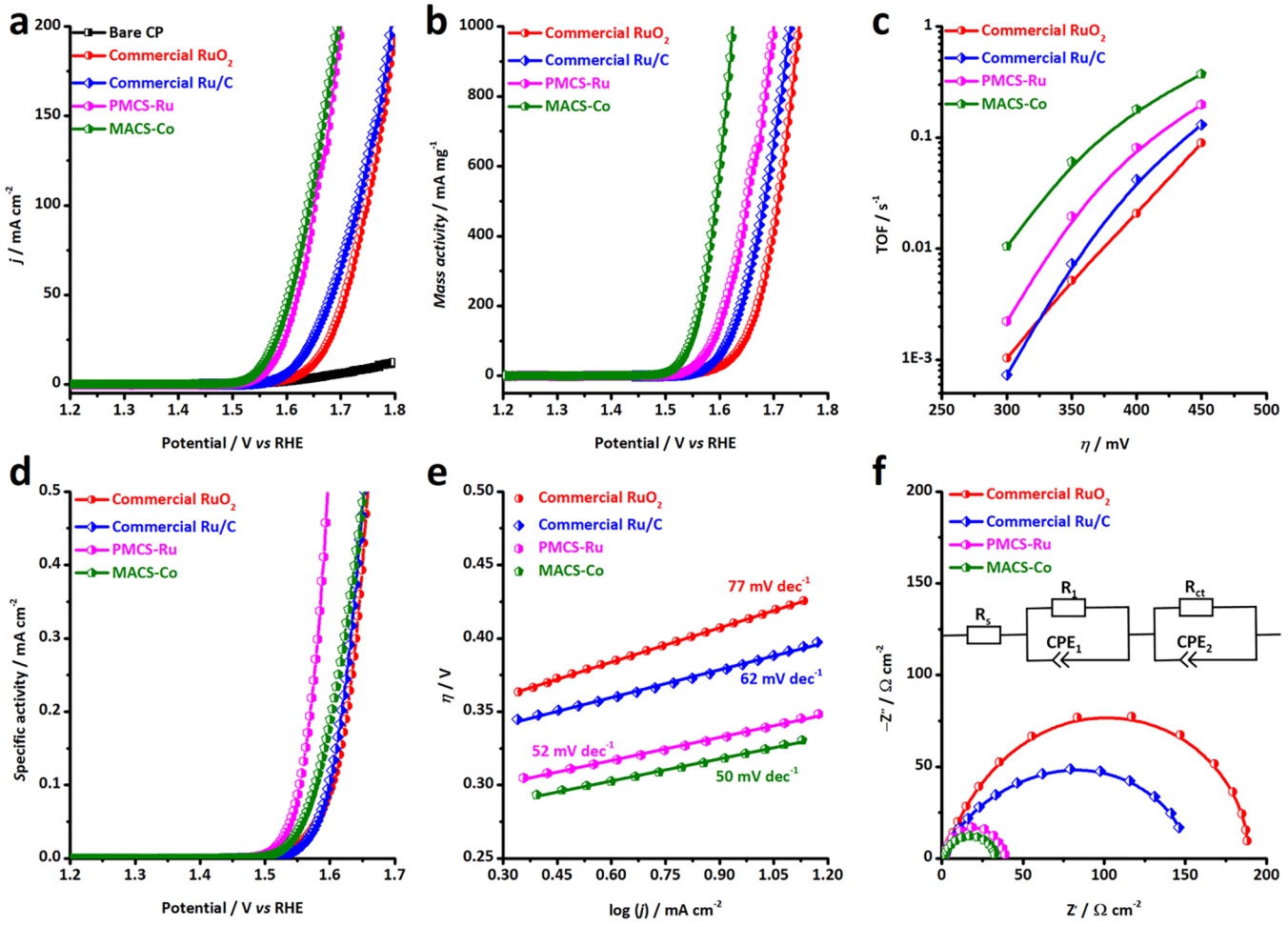

Figure 3. Electrocatalytic performance of all catalysts toward the OER. (a) Polarization curves. Scan rate: 5 mV s^{-1}. (b) Mass activities. (c) TOF values calculated at overpotentials of 300, 350, 400, and 450 mV. (d) Specific activities. (e) Tafel slopes. (f) EIS Nyquist plots recorded at 1.50 V vs RHE. Inset: the equivalent circuit model used for fitting. The solid lines are fitting curves. All measurements were carried out in 1.0 M KOH at room temperature.

monolayer coverage (3 nm thick) were obtained by rastering over an area of about 200 cm^2, in about 25 min.

Besides the CP substrate, both Co and Ru clusters were deposited as well on carbon-coated copper grids for scanning transmission electron microscopy (STEM) investigation. Panels a and b of Figure 1 show typical high-angle annular dark-field (HAADF) STEM images of the Co clusters obtained by MACS after 40 min of deposition. A bimodal ensemble of clusters can be observed, comprising larger clusters having a mean diameter of 3.2 nm and an areal density of 690−770 μm^{-2} (Figure 1c), surrounded by smaller clusters with a mean diameter of 1.8 nm that cover 25−32% of the surface (Figure 1d). The high-magnification image in Figure 1b also reveals that some bigger clusters have a core/shell structure, which may indicate that the Co clusters became at least partially oxidized when they were transferred from the MACS system into air. More high-resolution STEM (HRSTEM) images showing the partial oxidation of the ultrafine Co clusters are shown in Supporting Information Figure S1.

Figure 2a shows a representative HAADF-STEM image of the PMCS-Ru clusters. It is seen that these clusters are interconnected with each other and have an average size of 2.6 nm. Figure 2b displays the lattice spacing distribution measured from the high-resolution STEM images. By comparing with the lattice spacing of Ru metal (space group $P6_3/mmc$) and RuO_2 (space group $P4_2/mnm$), it is found that the majority of measured lattice distances correspond to the interplanar spacing of (011), (020), and (010) crystal planes of hexagonal Ru, indicating the metallic nature of the deposited Ru clusters. This was also corroborated by elemental mapping of Ru and oxygen of the clusters (Figure 2d−f), where oxygen primarily appears on the surface of the clusters with relatively low signal counts. This surface oxygen may result from the oxidation of Ru upon exposure in air.

To assess the electrocatalytic performance of the ultrafine Co and Ru clusters, the CBD processes were directly performed on a CP substrate (FuelCellStore). To improve the hydrophilicity and facilitate the anchoring of metal clusters, the CP substrate was pretreated in concentrated sulfuric acid, nitric acid, and water in sequence before the deposition. The electrocatalytic tests were conducted in an O_2-saturated 1.0 M KOH solution using cyclic voltammetry (CV), electrochemical impedance spectroscopy (EIS), and chronopotentiometry (CP). Prior to recording the CV curves, preactivation of electrodes was carried out by repetitive CV scans between 1.0 and 1.6 V vs reversible hydrogen electrode (RHE) at a scan rate of 100 mV s^{-1} until a steady state CV curve was obtained (Figure S2). During this process, the surface of catalysts may get oxidized, as reported in previous works.[24,25] Figure 3a shows the cathodic branches of the CV curves of MACS-Co and PMCS-Ru catalysts. For

DOI: 10.1021/acsaem.8b00111
ACS Appl. Energy Mater. 2018, 1, 3013−3018

comparison, we also measured the catalytic activity of commercially available Ru/C (FuelCellStore; Ru particle nominal size, 1−3 nm) and RuO_2 NPs (Alfa Aesar; nominal particle size, 25−35 nm) as well as a bare CP substrate. As seen in Figure 3a, the bare CP only shows a small anodic current up to 1.75 V vs RHE, indicating that CP is catalytically inactive for OER. The commercial RuO_2 NPs generate a benchmark anodic current density of 10 mA cm^{-2} at η_{10} = 420 mV, consistent with that reported for RuO_2 NPs or thin films in the literature.[24,25] The commercial Ru/C shows better OER activity than commercial RuO_2 NPs in the low-overpotential region with η_{10} = 380 mV. However, the catalytic current density generated by Ru/C is very close to that delivered by RuO_2 NPs in the high-overpotential region. In contrast, the PMCS-Ru exhibits substantially improved OER activity compared to both Ru/C and RuO_2 NPs, showing a large negative shift in the polarization curve (η_{10} = 330 mV). Remarkably, the MACS-Co clusters reveal OER activity that favorably compares to that of PMCS-Ru, requiring an overpotential of 320 mV to deliver 10 mA cm^{-2}, which outperforms many transition metal based OER catalysts in terms of apparent catalytic activity (Table S1), such as $Ni_xCo_{3-x}O_4$ nanowire (335 mV)[3], CoS−$Co(OH)_2$@$aMoS_{2+x}$/NF (380 mV)[4], FeO_x/CFC nanosheet (359 mV),[5] and NiCoP/C NP (330 mV).[6]

The mass activity of each catalyst is further compared (Figure 3b). Remarkably, MACS-Co shows a mass activity as high as 969 mA mg^{-1} at η = 390 mV, substantially higher than that of PMCS-Ru and other Ru-based control catalysts. The OER activities of all the catalysts were assessed and compared based on TOF. The TOF values were calculated assuming all metal species, no matter if they are on the surface or in the interior of catalysts, are active, which represent the lower limits of TOF.[26] Figure 3c shows the mass-based TOF values calculated at different overpotentials of 300, 350, 400, and 450 mV, which follow the same order as the observation of the apparent and mass OER activities (Figure 3a,b), namely, MACS-Co > PMCS-Ru > commercial Ru/C > commercial RuO_2. In particular, the TOF value of PMCS-Ru is 0.002 s^{-1} at η = 300 mV, while the TOF value of MACS-Co amounts to 0.01 s^{-1} at the same overpotential, higher than that of a number of Co-based OER catalysts, e.g., $Ni_xCo_{3-x}O_4$ nanowire (0.0007 s^{-1}),[3] Fe_3O_4@Co_9S_8/rGo NP (0.0045 s^{-1}),[27] and CoMnP NP (0.004 s^{-1}),[28] demonstrating better utilization of the catalysts derived from CBD.

Furthermore, the specific activities of all the catalysts are estimated to neutralize the effect of catalyst size difference. The specific activity was obtained by normalizing the catalytic current by the electrochemically accessible surface area (ECSA), which was estimated according to the double-layer capacitance measured in the non-Faradaic potential region (see Experimental Details in Supporting Information, Figure S4). As shown in Figure 3d, MACS-Co clusters, as platinum group metal free catalysts, show specific activity higher than that of both commercial RuO_2 and Ru/C catalysts; more remarkably, PMCS-Ru exhibits substantially higher specific activity than all other catalysts. This indicates that the ultrafine Co and Ru clusters prepared by CBD are intrinsically more active than the commercially available Ru-based OER catalysts.

The OER reaction kinetics of the catalysts were studied by Tafel analysis. Figure 3e shows the Tafel plots of MACS-Co, PMCS-Ru, and other commercial catalysts. The MACS-Co clusters show a Tafel slope of 50 mV dec^{-1}, substantially smaller than that of both commercial Ru/C and RuO_2 NPs, and even lower than that of PMCS-Ru clusters, indicating fast reaction kinetics. The Tafel impedance of MACS-Co was also derived from the impedance measurement, and the obtained Tafel slope matches well with that obtained from the polarization curve (Figure 3a) in the low current density region, but shows a higher value in the high current density region due probably to the influence of saturation of adsorbates[29] (Figure S3). The Tafel slope, to some extent, may provide useful information about the rate-determining processes at the reaction interface. According to the reaction pathway proposed by Krasil'shchikov,[30] the OER comprises the following sequential steps:

$$M + OH^- \rightarrow MOH + e^- \quad (1)$$

$$MOH + OH^- \rightarrow MO^- + H_2O \quad (2)$$

$$MO^- \rightarrow MO + e^- \quad (3)$$

$$2MO \rightarrow 2M + O_2 \quad (4)$$

The Tafel slopes of 50 mV dec^{-1} achieved by MACS-Co and of 52 mV dec^{-1} by PMCS-Ru indicate that the second electron transfer process, namely, step 3, is the rate-determining step (RDS) of the OER taking place on ultrafine clusters, in which case the discharge of OH^- (step 1) and subsequent chemical adsorption of OH^- (step 2) can be relatively easily accomplished. In fact, the fast reaction kinetics of Co and Ru clusters can be further corroborated by an EIS study. Figure 3f shows the Nyquist plots of MACS-Co, PMCS-Ru, and other commercial catalysts. Upon fitting the plots with the equivalent circuit model shown in Figure 3f inset, the charge transfer resistance (R_{ct}) was estimated to be 32 Ω for Co clusters and 37 Ω for Ru clusters (Table S2), which are both 4−5 times lower than that of commercial Ru/C (R_{ct} = 156 Ω) and RuO_2 NPs (R_{ct} = 186 Ω). This demonstrates that MACS-Co and PMCS-Ru clusters, as efficient electrocatalysts, drastically expedite the OER process compared to commercial Ru-based catalysts.

Long-term catalytic stability is an important indicator for OER electrocatalysts and is a crucial requirement for practical applications in water splitting. The catalytic stability of the MACS-Co, PMCS-Ru, commercial Ru/C, and RuO_2 catalysts was evaluated by chronopotentiometry at 10 mA cm^{-2}. As revealed in Figure 4, the MACS-Co and PMCS-Ru clusters show excellent catalytic stability, with overlapped behaviors that can afford 10 mA cm^{-2} without any degradation for at least 40 h. In contrast, the commercial Ru/C and RuO_2 NPs need a higher overpotential to maintain the same current density, and the overpotential needed to deliver 10 mA cm^{-2} increases by 70 mV for Ru/C and by 30 mV for RuO_2 NPs in 40 h, suggesting a degradation. Interestingly, the overpotential needed for PMCS-Ru clusters first increases and then gradually decreases by 10 mV after 40 h continuous electrolysis, ending up with an overpotential similar to that of the MACS-Co clusters. All these results indicate that the ultrafine Co and Ru clusters have outstanding catalytic stability for OER in alkaline solution, outperforming the state-of-the-art Ru/C and RuO_2 NPs.

In summary, we have prepared ultrafine Co and Ru clusters based on cluster beam deposition using the matrix assembly cluster source and the pulsed microplasma cluster source, respectively. We comprehensively investigated the electrocatalytic performance of Co and Ru clusters for the oxygen evolution reaction in alkaline solution: both cluster-based catalysts show results outperforming the commercially available

DOI: 10.1021/acsaem.8b00111
ACS Appl. Energy Mater. 2018, 1, 3013−3018

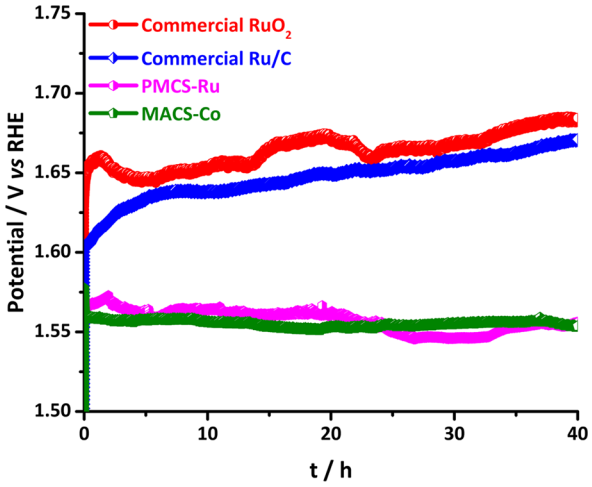

Figure 4. Chronopotentiometric curves recorded at 10 mA cm^{-2} in 1.0 M KOH at room temperature.

Ru/C and RuO_2 nanoparticles in terms of both mass and specific activities. In particular, the non-Pt group metal Co clusters deposited from MACS show high mass-based catalytic activity with a turnover frequency of 0.01 s^{-1} at an overpotential of 300 mV and a Tafel slope of 50 mV dec^{-1}, and the Ru clusters obtained from PMCS exhibit high specific activity of 0.30 mA cm^{-2} at an overpotential of 350 mV. Moreover, both Co and Ru clusters exhibit exceptional catalytic stability over a long term. Cluster beam deposition provides an effective and scalable approach to the synthesis of size-controlled transition or noble metal clusters which can be not only directly used as catalysts for electrochemical water splitting but also readily coupled with semiconductor photoelectrodes for photoelectrochemical water splitting. It is worth mentioning that CBD allows for achieving high catalyst mass loading while maintaining the small cluster size, given that the cluster size is determined by the cluster source prior to deposition and the catalyst film formation follows a "soft-assembling" mechanism, where the kinetic energy per atom of the impinging cluster is lower than its bonding energy, in such a way the cluster tends to maintain its original configuration (e.g., size) and the growth of the catalyst film occurs by the piling-up of clusters forming a highly porous, large specific area structure. Furthermore, CBD is also a potentially cost-effective technique, given that the utilization rate of raw materials in an optimized cluster deposition process is close to 100% and there is no cost (economic or environmental) of disposal of solvents or effluents, thereby showing great promise for catalyst preparation.

■ ASSOCIATED CONTENT

Supporting Information

The Supporting Information is available free of charge on the ACS Publications website at DOI: 10.1021/acsaem.8b00111.

Experimental details; HRSTEM characterization of Co clusters upon exposure in air; cyclic voltammograms of catalysts; Tafel impedance of Co clusters; determination of ECSA; performance comparison with other nonprecious OER electrocatalysts; summary of EIS fitting parameters (PDF)

■ AUTHOR INFORMATION

Corresponding Authors

*E-mail: r.e.palmer@swansea.ac.uk (R.E.P.).
*E-mail: lifeng.liu@inl.int (L.L.).

ORCID

Dehua Xiong: 0000-0002-4714-9019
Xian-Kui Wei: 0000-0003-4320-1120
Richard E. Palmer: 0000-0001-8728-8083
Lifeng Liu: 0000-0003-2732-7399

Present Addresses

#Department of Applied Science, Institute of Technology Tallaght, Dublin 24, Ireland.
▽State Key Laboratory of Silicate Materials for Architectures, Wuhan University of Technology, Wuhan 430070, People's Republic of China.

Notes

The authors declare no competing financial interest.

■ ACKNOWLEDGMENTS

We acknowledge the financial support of the European Commission through Horizon 2020 project "CritCat" (Grant Agreement No. 686053). L.L. acknowledges the support of the Portuguese Foundation of Science and Technology (FCT) through the FCT Investigator Grant (IF/01595/2014).

■ REFERENCES

(1) Hosseini, S. E.; Wahid, M. A. Hydrogen production from renewable and sustainable energy resources: Promising green energy carrier for clean development. *Renewable Sustainable Energy Rev.* **2016**, *57*, 850−866.

(2) Hong, W. T.; Risch, M.; Stoerzinger, K. A.; Grimaud, A.; Suntivich, J.; Yang, S.-H. Toward the rational design of non-precious transition metal oxides for oxygen electrocatalysis. *Energy Environ. Sci.* **2015**, *8*, 1404−1427.

(3) Yan, X. D.; Li, K. X.; Lyu, L.; Song, F.; He, J.; Niu, D. M.; Liu, L.; Hu, X. L.; Chen, X. B. From Water Oxidation to Reduction: Transformation from $Ni_xCo_{3-x}O_4$ Nanowires to NiCo/NiCO*x* Heterostructures. *ACS Appl. Mater. Interfaces* **2016**, *8*, 3208−3214.

(4) Yoon, T.; Kim, K. S. One-Step Synthesis of CoS-Doped *β*-$Co(OH)_2$@Amorphous MoS_{2+x} Hybrid Catalyst Grown on Nickel Foam for High-Performance Electrochemical Overall Water Splitting. *Adv. Funct. Mater.* **2016**, *26*, 7386−7393.

(5) Yan, F.; Zhu, C. L.; Wang, S.; Zhao, Y.; Zhang, X. T.; Li, C. Y.; Chen, Y. J. Electrochemically activated-iron oxide nanosheet arrays on carbon fiber cloth as a three-dimensional self-supported electrode for efficient water oxidation. *J. Mater. Chem. A* **2016**, *4*, 6048−6055.

(6) He, P. L.; Yu, X. Y.; Lou, X. W. Carbon-Incorporated Nickel−Cobalt Mixed Metal Phosphide Nanoboxes with Enhanced Electrocatalytic Activity for Oxygen Evolution. *Angew. Chem., Int. Ed.* **2017**, *56*, 3897−3900.

(7) Zheng, Y.; Jiao, Y.; Zhu, Y. H.; Cai, Q. R.; Vasileff, A.; Li, L. H.; Han, Y.; Chen, Y.; Qiao, S. Z. Molecule-Level g-C_3N_4 Coordinated Transition Metals as a New Class of Electrocatalysts for Oxygen Electrode Reactions. *J. Am. Chem. Soc.* **2017**, *139*, 3336−3339.

(8) Fan, K.; Chen, H.; Ji, Y. F.; Huang, H.; Claesson, P. M.; Daniel, Q.; Philippe, B.; Rensmo, H.; Li, F. S.; Luo, Y.; Sun, L. C. Nickel−vanadium monolayer double hydroxide for efficient electrochemical water oxidation. *Nat. Commun.* **2016**, *7*, 11981.

(9) Guan, J. Q.; Li, D.; Si, R.; Miao, S.; Zhang, F. X.; Li, C. Synthesis and Demonstration of Subnanometric Iridium Oxide as Highly Efficient and Robust Water Oxidation Catalyst. *ACS Catal.* **2017**, *7*, 5983−5986.

(10) Park, J.; Sa, Y. J.; Baik, H.; Kwon, T.; Joo, S. H.; Lee, K. Iridium-Based Multimetallic Nanoframe@Nanoframe Structure: An Efficient

DOI: 10.1021/acsaem.8b00111
ACS Appl. Energy Mater. 2018, 1, 3013−3018

and Robust Electrocatalyst toward Oxygen Evolution Reaction. *ACS Nano* **2017**, *11*, 5500−5509.
(11) Wegner, K.; Piseri, P.; Tafreshi, H. V.; Milani, P. Cluster Beam Deposition: A Tool for Nanoscale Science and Technology. *J. Phys. D: Appl. Phys.* **2006**, *39*, R439−R459.
(12) Kwon, G.; Ferguson, G. A.; Heard, C. J.; Tyo, E. C.; Yin, C.; DeBartolo, J.; Seifert, S.; Winans, R. E.; Kropf, A. J.; Greeley, J.; Johnston, R. L.; Curtiss, L. A.; Pellin, M. J.; Vajda, S. Size-Dependent Subnanometer Pd Cluster (Pd_4, Pd_6, and Pd_{17}) Water Oxidation Electrocatalysis. *ACS Nano* **2013**, *7*, 5808−5817.
(13) Nesselberger, M.; Roefzaad, M.; Fayçal Hamou, R.; Ulrich Biedermann, P.; Schweinberger, F. F.; Kunz, S.; Schloegl, K.; Wiberg, G. K. H.; Ashton, S.; Heiz, U.; Mayrhofer, K. J. J.; Arenz, M. The Effect of Particle Proximity on the Oxygen Reduction Rate of Size-Selected Platinum Clusters. *Nat. Mater.* **2013**, *12*, 919−924.
(14) von Issendorff, B.; Palmer, R. E. A New High Transmission Infinite Range Mass Selector for Cluster and Nanoparticle Beams. *Rev. Sci. Instrum.* **1999**, *70*, 4497−4501.
(15) Pratontep, S.; Carroll, S. J.; Xirouchaki, C.; Streun, M.; Palmer, R. E. Size-Selected Cluster Beam Source Based on Radio Frequency Magnetron Plasma Sputtering and Gas Condensation. *Rev. Sci. Instrum.* **2005**, *76*, 045103.
(16) Carroll, S. J.; Pratontep, S.; Streun, M.; Palmer, R. E.; Hobday, S.; Smith, R. Pinning of Size-Selected Ag Clusters on Graphite Surfaces. *J. Chem. Phys.* **2000**, *113*, 7723−7727.
(17) Hernandez-Fernandez, P.; Masini, F.; McCarthy, D. N.; Strebel, C. E.; et al. Mass-Selected Nanoparticles of PtxY as Model Catalysts for Oxygen Electroreduction. *Nat. Chem.* **2014**, *6*, 732−738.
(18) Palmer, R. E.; Cao, L.; Yin, F. Proof of Principle of A New Type of Cluster Beam Source with Potential for Scale-Up. *Rev. Sci. Instrum.* **2016**, *87*, 046103.
(19) Ellis, P. R.; Brown, C. M.; Bishop, P. T.; Yin, J.; Cooke, K.; Terry, W. D.; Liu, J.; Yin, F.; Palmer, R. E. The Cluster Beam Route to Model Catalysts and Beyond. *Faraday Discuss.* **2016**, *188*, 39−56.
(20) Oiko, V. T. A.; Mathieu, T.; Cao, L.; Liu, J.; Palmer, R. E. Production of Silver Nanoclusters Using a Matrix-Assembly Cluster Source with A Solid CO_2 Matrix. *J. Chem. Phys.* **2016**, *145*, 166101.
(21) Cai, R. S.; Jian, N.; Murphy, S.; Bauer, K.; Palmer, R. E. A New Method to Prepare Colloids of Size-Controlled Clusters From A Matrix Assembly Cluster Source. *APL Mater.* **2017**, *5*, 053405.
(22) Milani, P.; Iannotta, S. *Cluster Beam Synthesis of Nanostructured Materials*; Springer, 1999.
(23) Barborini, E.; Piseri, P.; Milani, P. A Pulsed Microplasma Source of High Intensity Supersonic Carbon Cluster Beam. *J. Phys. D: Appl. Phys.* **1999**, *32*, L105.
(24) Reier, T.; Oezaslan, M.; Strasser, P. Electrocatalytic Oxygen Evolution Reaction (OER) on Ru, Ir, and Pt Catalysts: A Comparative Study of Nanoparticles and Bulk Materials. *ACS Catal.* **2012**, *2*, 1765−1772.
(25) Özer, E.; Spöri, C.; Reier, T.; Strasser, P. Iridium(111), Iridium(110), and Ruthenium(0001) Single Crystals as Model Catalysts for the Oxygen Evolution Reaction: Insights into the Electrochemical Oxide Formation and Electrocatalytic Activity. *ChemCatChem* **2017**, *9*, 597−603.
(26) Zou, Z. X.; Zhang, Y. Noble metal-free hydrogen evolution catalysts for water splitting. *Chem. Soc. Rev.* **2015**, *44*, 5148−5180.
(27) Yang, J.; Zhu, G. X.; Liu, Y. J.; Xia, J. X.; Ji, Z. Y.; Shen, X. P.; Wu, S. K. Fe_3O_4-Decorated Co_9S_8 Nanoparticles In Situ Grown on Reduced Graphene Oxide: A New and Efficient Electrocatalyst for Oxygen Evolution Reaction. *Adv. Funct. Mater.* **2016**, *26*, 4712−4721.
(28) Li, D.; Baydoun, H.; Verani, C. N.; Brock, S. L. Efficient Water Oxidation Using CoMnP Nanoparticles. *J. Am. Chem. Soc.* **2016**, *138*, 4006−4009.
(29) Jaouen, F.; Lindbergh, G. Transient Techniques for Investigating Mass-Transport Limitations in Gas Diffusion Electrodes I. Modeling the PEFC Cathode. *J. Electrochem. Soc.* **2003**, *150*, A1699−A1710.
(30) Doyle, R. L.; Lyons, M. E. G. The Oxygen Evolution Reaction: Mechanistic Concepts and Catalyst Design. *Photoelectrochemical Solar Fuel Production*; Springer, 2016; Chapter 2, pp 41−104, DOI: 10.1007/978-3-319-29641-8_2.

DOI: 10.1021/acsaem.8b00111
ACS Appl. Energy Mater. 2018, 1, 3013−3018